PROCEEDINGS, 41st Workshop on Geothermal Reservoir Engineering
Stanford University, Stanford, California, February 22-24, 2016
SGP-TR-209

The Radiator-Enhanced Geothermal System (RAD-EGS): 3D modeling of heat transfer

Markus Hilpert[1], Bruce D. Marsh[1], Pete Geiser[2]

[1]Johns Hopkins University, Department of Earth and Planetary Sciences, Baltimore, Maryland, U.S.A.
[2]Global Geophysical Services, Denver, Colorado, U.S.A.
markus_hilpert@jhu.edu

Keywords: enhanced geothermal system, radiator, modeling

ABSTRACT

We have recently proposed a novel Enhanced Geothermal System (EGS) that addresses the difficulties of traditional EGSs. Conventional EGSs are typically not commercially successful because of the low thermal diffusivity of hot dry rock and the horizontal EGS geometry, which collectively hinder recharge in produced geothermal reservoirs. The challenge is to find or create sufficient rock permeability and to visualize accurately this permeability field to which a high efficiency heat exchanger can be tailored. RAD-EGS mimics naturally occurring hydrothermal systems, which contrary to EGS have frequently been proven to be economically sustainable. The RAD-EGS creates a vertically oriented heat exchanger or vane in the deep subsurface. This vane mimics a radiator in an internal combustion engine. Water is injected at the bottom of the vane and produced on top. Currently available subsurface imaging technology suggests that RAD-EGS be built in Hot Sedimentary Aquifers (HSA) using propellant fracking to create high permeability vane(s) in the plane defined by SH_{max} and S_1 (vertical). We have performed 3D heat transfer simulations in order to evaluate the RAD-EGS in a HSA. The simulations account for subsurface heterogeneity including the presence of underlying basement rock, an overlying confining layer, and an ambient horizontal hydraulic gradient. The simulated 3D fields of fluid pressure and velocity as well as temperature provide crucial information about the effluent temperature of the injected coolant and the pressure differential needed to maintain the circulation of the coolant as a function of time. These results allow evaluation of the efficiency of RAD-EGS. Our simulations indicate that the proposed induced upward flow in the vane can significantly prolong the lifetime of RAD-EGS when compared to downward flow. Specifically, produced fluid temperatures greater than 150°C that are required for commercial energy production can be maintained for significantly longer periods of time for upward flow. This suggests that mimicking a natural hydrothermal system is a successful EGS strategy. Recharge due to heat advection in the surrounding water-saturated aquifer also prolongs substantially the lifetime of the thermal reservoir. RAD-EGS does not suffer from fluid losses that can be substantial for EGS built in hot dry rock (HDR).

1. INTRODUCTION

We have recently proposed a novel Enhanced Geothermal System (EGS), the so-called Radiator EGS (RAD-EGS) (Geiser 2015a; Geiser 2015b). RAD-EGS addresses the difficulties of traditional EGSs, which have so far not succeeded in producing commercial amounts of energy (Tester et al. 2006). This failure can be attributed to the low thermal diffusivity of hot dry rock and the typically horizontal EGS geometry, which collectively hinder the thermal recharge in produced geothermal reservoirs. The RAD-EGS is designed to mimic naturally occurring hydrothermal systems, which contrary to conventional EGS have frequently been proven to be economically sustainable. In fact, almost all geothermal energy produced in the US stems from natural hydrothermal systems, primarily located in Hawaii and in California (The Geysers). The RAD-EGS creates a vertically oriented heat exchanger or a vane in the deep subsurface, mimicking a radiator in an internal combustion engine. Water is injected at the bottom of the vane and withdrawn on top.

A challenge of any EGS is to find or create sufficient rock permeability such that water can be injected and recovered at a higher temperature and at a sufficiently high flow rate. The vertical orientation of the heat exchanger is a crucial feature of RAD-EGS, because it takes advantage of the ambient stress field that can typically be found in the deep subsurface where a large-scale EGS would need to be built. At depths greater than about 700 m, the vertical stress S_1 is typically the maximum principal stress. Therefore, both natural and manufactured fractures tend to be vertical in the deep rock formations targeted by EGSs. Therefore, a vertically oriented heat exchanger is much easier to construct than a horizontally oriented one, and any existing fracture systems are an advantage rather than a liability. Another challenge is to visualize accurately the permeability field to which a high efficiency heat exchanger can be tailored. Currently available subsurface imaging technology suggests that RAD-EGS be built in Hot Sedimentary Aquifers (HSA) and not in volcanic or basement rocks, typically targeted when building EGS. This is because imaging of subsurface rock is based on accurate seismic velocity models, which are much easier to obtain in HSA. Another advantage of building RAD-EGS in a HSA is that thermal recharge may occur not only via heat conduction in the rock but also via heat advection by fluid flow in the surrounding HSA.

Numerical modeling has routinely been used to assist with the implementation of EGSs at specific field sites (Bachler and Kohl 2005; Dempsey et al. 2015) and to model real hydrothermal systems (Denlinger and Kovach 1981; Stimac et al. 2001; Fu et al. 2010; Dzikowski et al. 2016; Ratouis and Zarrouk 2016). Modeling has also been used to evaluate novel EGSs (Fairley, Ingebritsen et al. 2010), to examine forced and free convection in vertical permeable slots (Bataille et al. 2006), to study EGS in hot dry rock (Diersch et al. 1989; Watanabe et al. 2011), and to study chemical processes (Bachler and Kohl 2005).

Here we examine RAD-EGS generically and the sensitivity of RAD-EGS performance with regard to its design parameters. The specific objectives are (1) to analyze the fluid flow and heat transfer characteristics of RAD-EGS; (2) to illustrate that induced upward flow in the radiator vane is advantageous and that mimicking a natural hydrothermal system is therefore a promising strategy for

constructing a successful EGS; and (3) to illustrate that thermal recharge through heat advection can extend the lifetime of RAD-EGS substantially. In order to accomplish these objectives, we have performed 3D heat transfer simulations.

2. MATHEMATICAL MODEL

2.1 General modeling approach

We used COMSOL™ to create a numerical model of RAD-EGS that simulates coupled heat and mass transfer. The model accounts for the presence of a hot sedimentary aquifer (HSA), an underlying typically less permeable basement rock, a relatively permeable radiator vane heat exchanger, a confining layer above the HSA, and an injection and withdrawal well (**Fig. 1**). We used a modeling approach that represents fractured rock by an effective porous medium, because we did not intend to make predictions for an actual, well-characterized field site, where the 3D permeability fields (or the fracture geometry) of the stimulated and stimulated rock might be available. This approach can be expected to perform well as long as the fracture spacing is sufficiently dense (Freeze and Cherry 1979) and as long as the vane is localized enough to be described simply as a well defined region of high permeability.

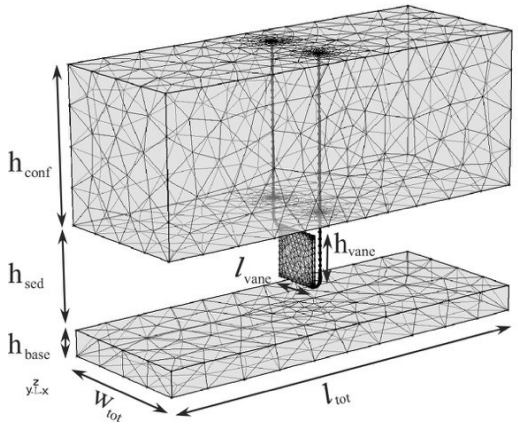

Figure 1: Sketch of the numerical model used to represent RAD-EGS in a HSA, which is underlain by less permeable basement rock and overlain by a confining layer. The cuboid that is connected to the two wells represents the highly permeable radiator vane. Shown is a sample coarse discretization of the domain. For better visualization, the discretization of the HSA is not shown.

Flow in the fractured, porous medium is therefore described by Darcy's law,

$$\vec{u} = -\frac{\kappa}{\mu}\left(\vec{\nabla} p + \rho_f g \vec{\nabla} z\right) \tag{1}$$

and the mass conservation equation for steady-state flow,

$$\vec{\nabla} \cdot \rho_f \vec{u} = 0 \tag{2}$$

where ρ_f is the fluid density, g is the gravitational acceleration, μ is the dynamic viscosity of the fluid, κ is the effective permeability of the fractured rock, and $\vec{u}$ is the Darcy velocity. Heat transfer in the fractured porous medium is described by an energy equation,

$$\bar{C}\frac{\partial T}{\partial t} + C_f \vec{u} \cdot \vec{\nabla} T = \nabla \cdot (\bar{k} \nabla T) \tag{3}$$

where

$$C_f = \rho_f c_{f,p} \tag{4}$$

is the volumetric heat capacity of the fluid (water), $c_{f,p}$ is the specific heat capacity of the fluid, T is temperature,

$$\bar{C} = (1-\varepsilon)\rho_r c_{r,p} + \varepsilon \rho_f c_{f,p} \tag{5}$$

is the volumetric heat capacity of the fluid-saturated rock, ρ_r is the density of the rock, $c_{p,r}$ is specific heat capacity of the rock, ε is the volume fraction of the porous, fractured rock,

$$\bar{k} = (1-\varepsilon)k_r + \varepsilon k_f \tag{6}$$

is the thermal conductivity of the fluid-saturated rock, k_f is the thermal conductivity of the fluid, and k_r is the thermal conductivity of the rock. The overbars indicate volume averaging based on the assumption of local thermal equilibrium between the fluid and the rock.

Water is modeled as a compressible and superheated fluid, the density ρ_f, heat capacity $c_{,f,p}$, dynamic viscosity μ and thermal conductivity k of which are a function of temperature T. We furthermore make the simplifying assumption that water is present in liquid form, even if the boiling point of water under atmospheric conditions, 100 °C, is exceeded. While this assumption is justified in

the deep subsurface because of the high fluid pressures, water can be expected to flash into steam in the production well, a process not accounted for by our modeling approach.

Flow in the wells is simulated based on the Darcy-Weisbach equation for pipe flow, $\frac{dp}{dz} = f_D \frac{\rho_f u_w^2}{2D}$ where dp/dz is the pressure gradient, f_D is the Darcy friction factor, u_w is the average fluid velocity in the well, and D is the hydraulic diameter of the pipe. In terms of mass flow rate $\dot{m}$, the pressure drop in the wells is given by

$$\frac{dp}{dz} = \frac{f_D}{4\rho_f \pi^2 R_w^5} \dot{m}^2 \tag{7}$$

where R_w is the well radius. For the turbulent flows that typically occur in geothermal applications, we tentatively use the Blasius correlation equation for the friction factor, $f_D = 0.316\ \mathrm{Re}^{-1/4}$ where $\mathrm{Re} = v_w\, 2\, R_w\, \rho_f / \mu$ is the Reynolds number.

2.2 Geometry

In the horizontal directions (x and y), the domain is centered around the axes of origin. In the vertical direction (z, axis pointing upward), the plane $z = 0$ forms the interface between the basement rock and the HSA. Basement rock is present in the cuboid domain defined by $-l_{tot}/2 \le x \le l_{tot}/2$, $-w_{tot}/2 \le y \le w_{tot}/2$ and $-h_{base} \le z \le 0$ where l_{tot} is the total length of the domain, w_{tot} is the total domain width, and h_{base} is the height (or thickness) of the basement rock layer. The vane itself is present in a cuboid domain defined by $-t_{vane}/2 \le x \le t_{vane}/2$, $-l_{vane}/2 \le y \le l_{vane}/2$ and $\bar{z}_{vane} - h_{vane}/2 \le z \le \bar{z}_{vane} + h_{vane}/2$ where t_{vane} is the thickness of the vane, l_{tane} is the length of the vane, h_{vane} is the vane height, and $\bar{z}_{vane}$ is the center of the vane in the vertical direction. The non-stimulated HSA is present in a cuboid domain defined by $-l_{tot}/2 \le x \le l_{tot}/2$, $-w_{tot}/2 \le y \le w_{tot}/2$ and $0 \le z \le h_{sed}$ except for the region in which the vane is present. The confining layer on top is present in a cuboid domain defined by $-l_{tot}/2 \le x \le l_{tot}/2$, $-w_{tot}/2 \le y \le w_{tot}/2$ and $h_{sed} \le z \le h_{sed} + h_{conf}$.

2.3 Boundary and initial conditions

The following boundary conditions are applied:

1. At the head of the production well, a constant upward mass flow rate $\dot{m}$ is applied mimicking the action of a pump. An outflow thermal boundary condition $\partial T/\partial z = 0$ is applied to the temperature of the borehole fluid (i.e., the fluid ascends rapidly enough, once established, not to cool).
2. At the head of the injection well, the same flow rate with opposite sign, $-\dot{m}$, is applied. The incoming fluid temperature is held at a constant value T_{in}, the injection temperature.
3. At the top of the domain ($z = h_{sed} + h_{conf}$), a no-flux fluid boundary condition, $q = 0$, is applied, and the temperature is set to a constant value T_t which is the temperature of the ground surface and on the order of T_{in}.
4. At the bottom of the domain ($z = -h_{base}$), a no-flux fluid boundary condition is applied, and the temperature is set to a constant value determined by the background geothermal gradient $dT/dz < 0$, that is, $T = T_t + |dT/dz|\,(h_{base} + h_{sed} + h_{conf})$.
5. On the two far field or confining sidewalls ($y = \pm\ w_{tot}/2$), a no-flux boundary condition is applied. Lateral thermal insulation, $\partial T/\partial y = 0$, is assumed.
6. At the domain inlet ($x = -\ l_{tot}/2$), a Darcy velocity is prescribed according to an assumed hydraulic head gradient i. The temperature at each level is assumed to be constant, but varies vertically as determined by the background geothermal gradient, $T(z) = T_t + |dT/dz|\,(h_{base} + h_{sed} - z)$.
7. At the domain outlet ($x = l_{tot}/2$), a Darcy velocity is prescribed according to an assumed hydraulic head gradient i. For temperature, an outflow boundary condition $\partial T/\partial x = 0$ is applied.
8. At the domain inlet of the basement rock layer ($x = -\ l_{tot}/2$), we also prescribe a Dirichlet boundary condition for the hydraulic head, because otherwise only Neuman boundary conditions for hydraulic head would be prescribed on the boundaries of the entire numerical domain, which would not allow for a unique solution for hydraulic head.

The following initial conditions were applied: (1) For fluid flow, the hydraulic head is assumed to decrease linearly along the x-direction according to the background hydraulic gradient i, that is, $H(x,y,z,t=0) = H_l - i(x + l_{tot}/2)$ where H_l is a constant hydraulic head. (2) The background geothermal gradient determines the initial temperature field in the entire domain, $T(z) = T_t + |dT/dz|\,(h_{sed} + h_{conf-} - z)$.

3. BASELINE SIMULATION PARAMETERS

3.1 Geometry

We created a model to simulate a simple, but realistic representation of a RAD-EGS installed in a HSA similar to the Raton Basin in Colorado. In that region, geothermal gradients of 56°C/km and even higher have been observed, with granitic basement rock beginning at depths between 4 and 9 km. Assuming a ground surface temperature of 20°C and basement rock to begin at a 5-km depth, the rock temperature at that depth is 300°C. We assumed the HSA to have a height of $h_{sed} = 2$ km. Therefore the height of the confining layer is

h_{conf} = 3 km. The modeled height of the underlying basement rock is h_{base} = 0.5 km. For this height, we expect the effects of imposed temperature boundary conditions on RAD-EGS performance to be negligible.

The vane is assumed to be large enough to allow for commercial energy production. It has a height and length of 1 km. The lateral extent of an actual artificially stimulated fracture zone, t_{vane}, is not known exactly. In the Sandia experiments (Cuderman 1984), two vertical fractures propagated from the borehole into surrounding rock. We consider it more likely that, under the proposed cycling of the strain rate dp/dt during propellant stimulation, steeply dipping mode 2 (shear) fractures will form making an acute angle with S_1 and whose intersection parallels S_2. This would be advantageous as shear fractures are self-propping. We currently do not know how far laterally from the well the shear fractures will reach into the surrounding wall rock. The reach of these fractures provides a measure for w_{vane}. The wider the vane, the more water is be able to flow through a larger volume of basin rock (HSA), and thus the more heat that can be harvested efficiently due to pore-water advection; instead of heat being recharged purely by conduction.

The thickness is determined by the assumption that propellant fracking can be used to create new fractures that extend 30 m outward from each borehole.. The entire vane can therefore be constructed by drilling a 'picket fence' family of vertical stimulation wells each, say, 60 m apart (a stack of horizontal wells also may work) into a planar rock area, which is spanned by the vectors of vertical stress S_1 and maximum horizontal stress Sh_{max}. Propellant is deflagrated in each well in several stages in order to create the vane defined by a highly interconnected permeability field. We assumed the vertical position of the centroid of the vane, $\bar{z}_{vane}$, to be centered in the HSA, i.e., $\bar{z}_{vane}$ = 1 km.

3.2 Thermodynamic material properties

The specific heat at constant pressure of the fractured rocks is assumed to be c_p = 1,200 J kg^{-1} K^{-1} (JASON 2013). The thermal conductivity of rock is assumed to be k_p = 3 W m^{-1} K^{-1} (JASON 2013). **Table 1** summarizes the material properties.

3.3 Nonstimulated-rock permeabilities

We assume the HSA to consist of sandstone, even though this, strictly speaking, need not be the case. According to Dingman (2002) sandstone has a hydraulic conductivity K_h that varies between 10^{-5} and 1 m/day. Since $K_h = \kappa \rho_f g / \mu$, the permeability κ of sandstone varies between 10^{-17} and 10^{-12} m^2 (assuming ρ_f = 1,000 kg/m^3 and $\mu = 10^{-3}$ kg/m-s). In our simulations, we assumed a HSA that is relatively permeable such that the geothermal reservoir can be recharged via advective heat flow, i.e., $\kappa_{sed} = 10^{-14}$ m^2. The porosity, is assumed to be ε_{sed} = 0.08. For the basement rock, we used a permeability 1,000 times smaller than the one defining the HSA, i.e., κ_{base} = 10^{-17} m^2, and the porosity is set at ε_{base} = 0.01, and these same values are also used for the overlaying confining layer.

3.4 Vane permeability

Little is currently known about the effective overall permeability (κ_{vane}) of the fractured rock stimulated by propellant fracking, i.e., the vane permeability. In making such an estimate there are two obvious approaches to follow:

1. The permeability can be assumed to be similar to that found in fault zones where natural hydrothermal systems already exist, which are the systems RAD-EGS seeks to emulate. We therefore suggest using a value of $\kappa_{vane} = 10^{-11}$ m^2 = 10 Darcy, which is estimated by Caine and Tomusiak (2003) for fault zones in the Colorado Rocky Mountain Front Range. And also, as based on anecdotal industrial evidence (ATK Orbital, private communication), the width of the stimulated vane is assumed to be t_{vane} = 60 m.

2. A second, perhaps more mechanistic approach of estimating κ_{vane}, consists of making assumptions about the aperture and number of the induced fractures and then using a fissure model to infer κ_{vane} (see **Figure 2**). Fissure models for fractured rock are based on the fact that the average flow velocity in a plane fissure is given by $v = -\frac{1}{\mu}\frac{b^2}{12}\left(\frac{\partial p}{\partial z} + \rho_f g\right)$ where b is the aperture of the fissure. Assuming that the flow in the vane is solely explained by flow in N_f induced parallel fractures, the average Darcy velocity in the vane is given by $q_{vane} = \frac{N_f Q_f}{t_{vane} l_{vane}}$ where $Q_f = v b l_{vane}$ is the volumetric flow rate in a single fissure. An effective permeability κ_{vane} of the vane is then defined according to the following equation: $q_{vane} = -\frac{\kappa_{vane}}{\mu}\left(\frac{\partial p}{\partial z} + \rho_f g\right)$. By combining these various equations derived one can now show that

$$\kappa_{vane} = \frac{N_f}{12}\frac{b^3}{t_{vane}} \tag{8}$$

In order to estimate the unknown model parameters b and N_f, we first assume that the apertures of induced fractures are on the order of the apertures estimated by (Caine and Tomusiak 2003) for the aforementioned fault zones, i.e., b = 10, 100 or 1,000 μm. We optimistically assume b = 1,000 μm. We furthermore assume that only one fracture is generated, N_f = 1. This assumption is justified far away from the well in which the propellant is deflagrated as shown in the Sandia propellant fracturing experiments (e.g., Cuderman 1984). With t_{vane} = 60 m, one now obtains $\kappa_{vane} = 1.4 \times 10^{-12}$ m^2 = 1.4 Darcy. For

smaller w_{vane} values, κ_{vane} increases, whereas the transmissivity of the vane $T_{vane} = \kappa_{vane} t_{vane} = N_f b^3 / 12$ remains constant.

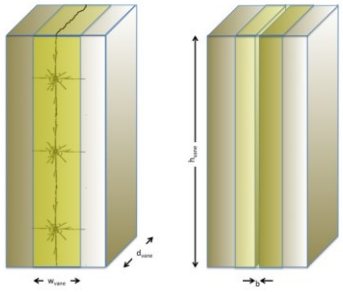

Figure 2: In our model, the actual stimulated fracture zone (LHS) of approximate thickness t_{vane} = 60 m is represented by a cuboid region with a uniform enhanced permeability κ_{vane} (RHS). This permeability is chosen based on the assumption that the actual fracture system can be represented by a single plane fracture with an effective aperture b = 1 mm chosen according to a fault zone study by (Caine and Tomusiak 2003).

Interestingly the two estimates for κ_{vane} are only one order of magnitude apart, which is not much for permeability when compared on the usual logarithmic scale. Herein, we conservatively assume that the permeability is determined by the second consideration, i.e., κ_{vane} = 1.4 × 10^{-12} m^2. We note, however, that this κ_{vane} value would be an overestimate should propellant fracking not result in a fracture, which continuously connects the bottom with the top of the vane. Nevertheless, regardless of the actual style of fractures possible to produce presently with propellant fracking, these calculations place critical constraints on the overall hypothetical vane size, shape, and permeability necessary in order to produce a satisfactory EGS.

Table 1: Overview of parameter values used in the baseline simulation of RAD-EGS.

Property	Symbol	Value	Units
Height of total domain	h_{tot}	5.5	km
Height of HAS	h_{sed}	2	km
Height of basement rock	h_{base}	0.5	km
Height of confining layer	h_{conf}	3	km
Height of vane	h_{vane}	1	km
Vertical position of vane centroid	$\bar{z}_{vane}$	1	km
Length of total domain	l_{tot}	8	km
Thickness of vane	t_{vane}	60	m
Width of total domain	w_{tot}	3	km
Length of vane	l_{vane}	1	km
Well radius	R_w	7.5	cm
Flow rate	$\dot{m}$	100	kg/s
Density of rock matrix	ρ_r	2,500	kg/m^3
Porosity of fractured HSA and vane	ε_{sed}	8%	-
Porosity of basement rock and confining layer	ε_{base}	1%	-
Thermal conductivity of porous rock	k_p	3.0	W/m-K
Specific heat of porous rock	c_p	1,200	J/kg-K
Permeability of HAS	κ_{sed}	10^{-14}	m^2
Permeability of basement	κ_{base}	10^{-17}	m^2
Permeability of vane	κ_{vane}	1.4 x 10^{-12}	m^2
Permeability of confining layer	κ_{base}	10^{-17}	m^2
Geothermal gradient	dT/dz	56	°C/km
Injection temperature	T_{in}	20	°C

4. SIMULATION RESULTS

4.1 Overview

Overview of intentions of the various simulations:

1. Baseline simulation of RAD-EGS with reasonable parameter estimates.
2. RAD-EGS for downward flow to show that the mimicking a natural hydrothermal system is reasonably good.
3. Larger and smaller vane permeabilities employed to explore onset of thermal convection.
4. Larger and smaller permeability in the rock surrounding the vane in order to elucidate the effects of advective recharge and the density-driven escape of the injected cold fluid into deeper rock layers.

5. Varying of background hydraulic gradient to explore the importance of thermal recharge by the natural background flow of groundwater.

Table 2 summarizes all simulations presented herein.

Table 2: Overview of simulations in which we varied selected parameters of the baseline simulation. Non-listed simulation parameters are taken from Table 1. A hyphen indicates that the baseline value from Table 1 is used.

	Baseline	Downward flow in vane	Higher flow rate	Higher vane permeability	Faster background flow	Higher HSA permeability	Lower HSA permeability
κ_{sed}	–	–	–	–	–	10^{-13} m^2	5×10^{-15} m^2
κ_{vane}	–	–	–	1.1×10^{-11} m^2	–	–	–
$\dot{m}$	–	−100 kg/s	200 kg/s	–	–	–	–
i	–	–	–	–	5%	–	–

4.2 Baseline simulation

For the baseline simulation, a sharp coolant front moves progressively upward through the vane while harvesting heat from the country rock as illustrated in **Figure 3**. In a similar fashion, a diffusive cooling front moves laterally into the wall rock and develops a halo around the vane. The speed of the vertical-trending cooling front is roughly determined by a balance between the extracted heat and rate of recharge by heat conduction in the HSA and heat advection via the natural background flow of groundwater.

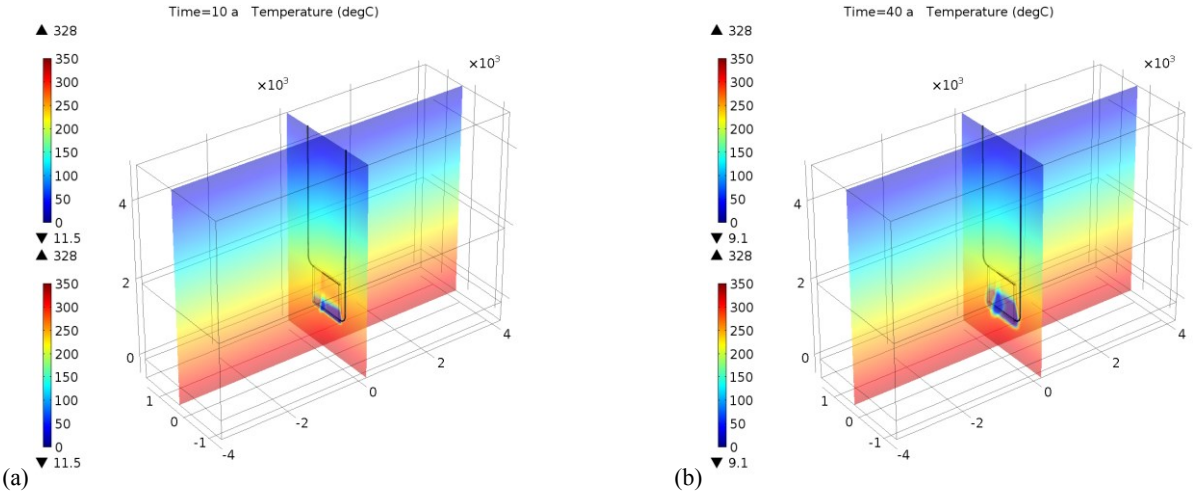

Figure 3: Temperature field for the base line simulations (a) 10 and (b) 40 years into operation of RAD-EGS.

The observed large-scale or overall temperature field is consistent with the fluid velocity field within the vane shown in **Fig. 4.** In the vane, the fluid flows relatively uniformly upward. The vertical variations can be attributed to the dependence of fluid density on temperature, which according to fluid mass conservation in the vane (neglecting advective recharge for the moment) causes the cold fluid below the cooling front in the vane to flow slower than the warmer fluid above the cooling front.

It is clear that a large-scale convective instability occurs in the wall rock surrounding the vane as illustrated in **Fig. 4**. This large-scale flow is due, in effect, to sidewall cooling (or heating) of the saturated porous sedimentary layers by the vane. This produces a horizontal temperature gradient, which induces a lateral density gradient in the fluid, inducing convection. This style of flow has been analyzed by Cheng and Minkowycz (1977) and Nield and Bejan (2006). Although in many similar convective flows, as in heating a layer from below, the existence and vigor of the flow is a matter of thermal stability as measured by the Rayleigh number (Ra) and the flow only occurs if the vertical temperature gradient exceeds a certain level, here with a horizontal thermal gradient the flow is intrinsically unstable at all temperature gradients. All measures of the flow, including, for example, the spatial scale, velocity, and heat transfer are given by the magnitude of the associated Ra, which is, in turn, determined by the rate of heat transfer induced by the vane flow. The governing Rayleigh number is:

$$\mathrm{Ra} = \frac{\kappa\rho^2 c_p g\beta(T_w - T_\square)\, h}{k_{eq}\,\eta} \tag{9}$$

where the lateral temperature gradient is from the vane wall (T_w) to the far field (T_{00}), and is averaged over the effective vane thermal height of h. With the magnitude of Ra increases with increasing height, the strength of this induced flow also increases, which enhances the recharge of thermal energy to the vane area.

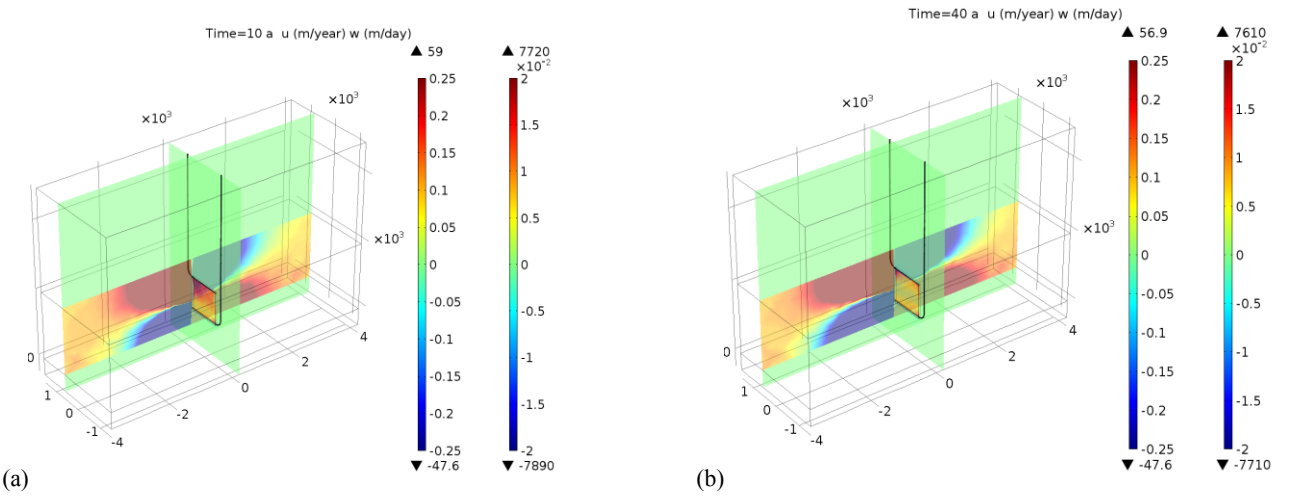

Figure 4: Velocity field for the base line simulations (a) 10 and (b) 40 years into operation of RAD-EGS. In the slice that cuts through the vane and both wells, the vertical fluid velocity is shown, where red and blue indicate upward and downward flow, respectively (range shown: –0.25 to +0.25 m/day). In the longitudinal slice, the horizontal fluid velocity is shown, where red and blue indicate flow to the right and left, respectively (range shown: –2 to +2 cm/day).

For the baseline simulation, the reservoir is harvested in a sustainable fashion (**Fig. 5).** After 4 years of operation, the effluent temperature reaches a maximum value of 240°C. After 40 years of operation, the effluent temperature is still substantial, namely 230°C, which would still allow for commercial electricity production. The pressure difference between injection and production wells is initially about 20 bars. After 5 years, this pressure difference becomes negative. This could be related to the fact that the colder and denser water in the injection well can spontaneously displace the warmer and lighter water in the production well. This line of reasoning does not apply to the first 4 years of RAD-EGS operation, because the water in the production well has not yet been heated up by the hot water received from the bottom of the vane. After having reached its minimum value, the pressure difference gradually increases to a value of about 20 bar after 40 years. This increase could be related to a general cooling of the rock, which increases the dynamic viscosity μ and hence the viscous pressure drop or overall drag to increase.

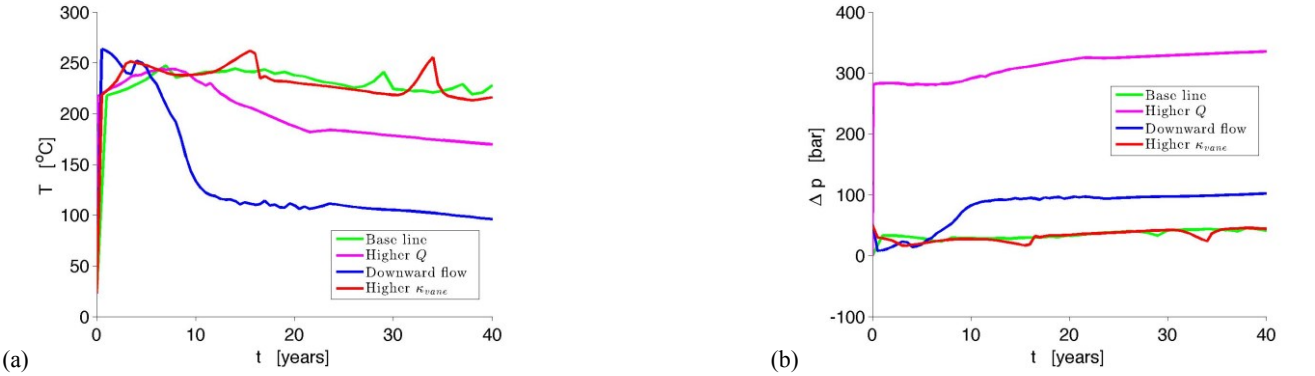

Figure 5: (a) Effluent temperature and (b) pressure difference between the heads of the injection and production wells for the first 4 simulation scenarios from Table 2.

4.3 Higher vane permeability

For a larger vane permeability κ_{vane}, a convective instability occurs within the vane itself as illustrated in **Figure 6**. This instability can be explained by theoretical stability analyses on free thermal convection in a horizontally layered, fluid-saturated porous medium that is held at a temperature T_2 at the bottom and at a temperature $T_1 < T_2$ on top. The criterion for the onset of convection can be expressed in terms of the Rayleigh number:

$$\mathrm{Ra} = \frac{\kappa \rho_f^2 c_{f,p}\, g \beta (T_1 - T_2)\, h}{\bar{k}\, \mu} \tag{10}$$

where β is the thermal expansion coefficient of the fluid, and h is the thickness of the porous layer (Malkovsky and Pek 2015). Convection occurs if Ra > 4π2 ≈ 39 (Lapwood 1948). The fact that the vane is of finite thickness and not an infinite horizontal sheet will affect this critical value. Murphy 's analysis of convection in a slot (vane) filled with porous material shows that the governing Rayleigh number (Ra*) is now given by Ra* = Ra (d/h) 2, where d is the thickness of the slot and h is the slot height (Murphy 1979). Convection occurs when Ra* exceeds a value of about 10 and attains steady state in a time given by $\sim d^2/D_r$, which is the conductive time scale for the slot or vane where D_r is the rock thermal diffusivity. Assuming the conditions are met for convection to occur, for this

vane of half thickness 30 m, the time to attain steady state is about 30 years, which suggests that for most of the time of study (~40 years) the convection will be intermittent or pulsatile.

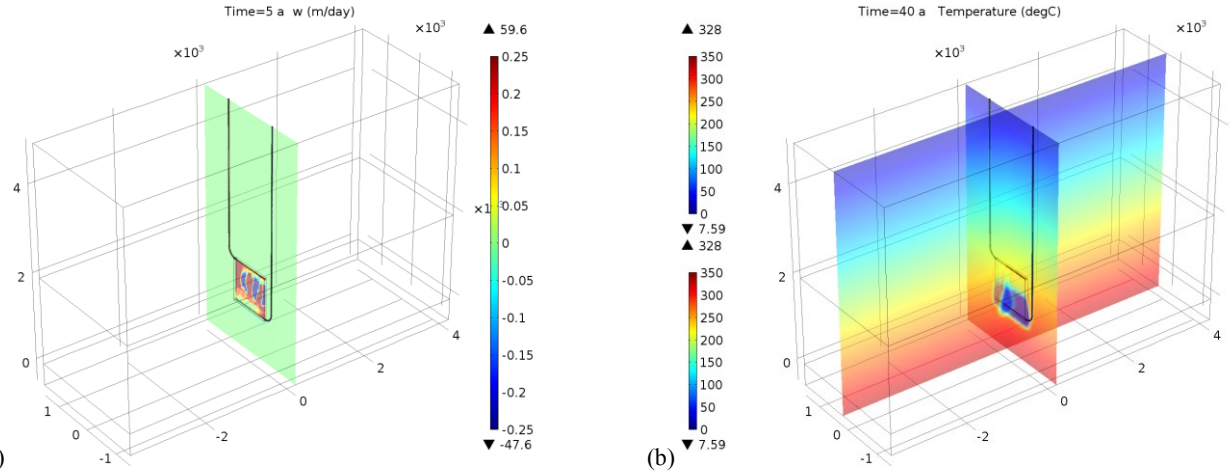

Figure 6: Simulation of RAD-EGS for higher vane permeability. (a) Velocity field. (b) Temperature field. The cooling front is sharp despite the convective instability.

Within geothermal applications, rock layers with high geothermal gradient *dT/dz* are often targeted, because these layers are associated with high rock temperature at relatively shallow depths. In terms of *dT/dz*, the Rayleigh number becomes

$$\mathrm{Ra} = \frac{\kappa_{vane}\,\rho_f^2 c_{f,p}\,g\,\beta\,\frac{dT}{dz}\,h_{vane}^2}{\bar{k}\,\mu} \tag{11}$$

Among the properties in the Rayleigh number, κ_{vane}, *dT/dz* and h_{vane} appear to be the most variable ones in our geothermal application, which uses water as the circulated fluid.

The boundary conditions used in these analyses do not apply exactly, because in RAD-EGS a net upward flow is created or forced due to the injection of the cooled fluid. The critical Rayleigh number for onset of convection increases with the flow rate (Homsy and Sherwood 1976; Jones and Persichetti 1986). However, the results of these studies do not directly apply to RAD-EGS for the following reasons:

1. The fluid is injected uniformly across the bottom of the porous medium layer, an assumption that cannot be made for the vane.
2. The temperature is uniform and highest at the bottom of the domain. However, in RAD-EGS the lowest temperature occurs at the fluid injection point at the bottom of the vane, and temperature is not uniform at the bottom due to the injection of relatively cold fluid.
3. In RAD-EGS, the porous medium layer, i.e., the vane, is not of infinite extent in the two horizontal directions. The vane can rather be assumed to be a vertical slot. In such a domain, the onset of convection is along the lines of the free-convection as mentioned already above (e.g., Murphy, 1979).

Currently, no theoretical stability analyses are available that use exactly the boundary conditions of RAD-EGS. It is therefore reasonable to assume tentatively that convection in the vane begins occurring once Ra* > ~10, the result for free convection in a slot. Calculating Ra requires estimating fluid properties, all of which depend on the fluid temperature, which is highly nonuniform due to the injection of cold water. If we evaluate the fluid properties at the injection temperature T_{in} = 20°C, we obtain Ra = 133 and 1,051 for the baseline and the high vane-permeability simulations, respectively, which for (*d*/*h*) = (60/1000) gives Ra* of about 0.5 and 4. However, if we evaluate the fluid properties at a typical background rock temperature of T = 200°C, we obtain Ra = 771 (Ra* ~ 3.0) and 6,056 (Ra* ~22). Although these values are not especially large, they are sufficiently close to the critical value of Ra*~ 10 to expect that this system will undergo free convection as seen in the numerics.

4.4 Induced downward flow

The flow and temperature fields for induced downward flow differ significantly from those for induced upward flow. The relatively cold water that is injected from the top of the vane does not uniformly flow downward as shown in **Fig. 7**. Instead it forms, in effect, a cold plume and flows downward only next to the injection point, and the flow field is almost at steady state, very much unlike the transient flow field that occurs during thermal convection. The region in which fluid flows downward with a high velocity represents a preferential flow channel for the injected could water, or a hydraulic short circuit. Consequently heat is harvested from only a small portion of the vane, and early breakthrough of the cold water occurs.

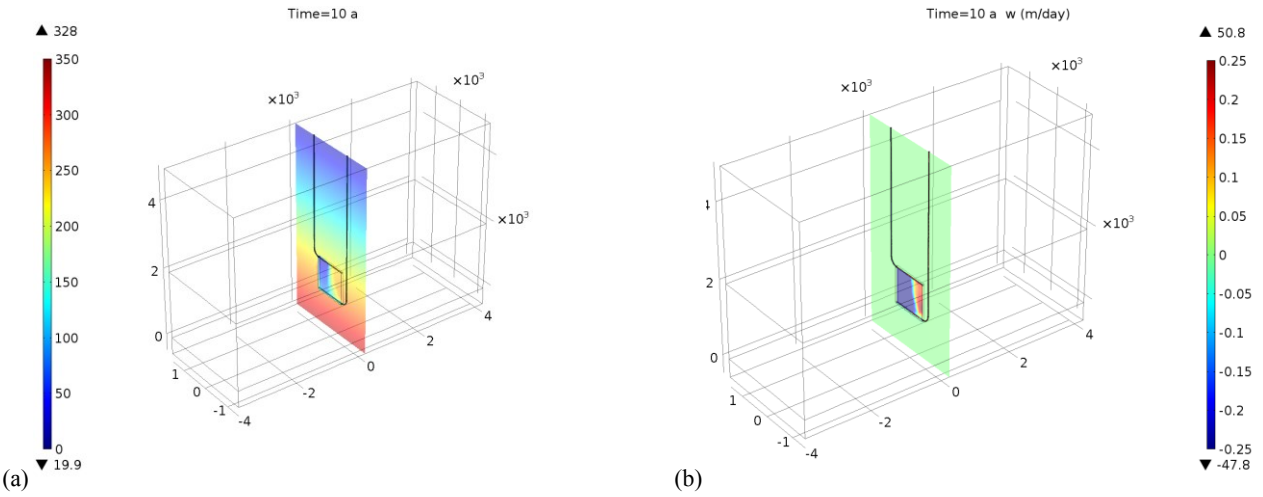

(a) (b)

Figure 7: Simulation of a "RAD-EGS" in which downward flow is induced in the vane. (a) Vertical flow velocity in a slice through the vane 10 years after operation of RAD-EGS started. (b) Temperature in the same slice. This modus of operation is not recommendable, because a persistent preferential flow channel next to the injection point on top of the vane directs cold water quickly to the bottom of the vane.

4.5 Higher flow rate

For a flow rate twice as high as the one from the baseline simulation, $\dot{m}$ = 200 kg/s, the performance of RAD-EGS becomes unattractive in several respects. Firstly, the production temperature drops quickly (after 9 years) below the critical threshold for commercial production of electrical energy, which is 150°C (**Fig. 5a**). Thus the lifetime is significantly shortened. Moreover, a significant pressure difference, on the order of 300 bar, is necessary in order to establish the higher flow rate (**Fig. 5b**). This increases the power needed to operate the pumps to a level likely making RAD-EGS uneconomical.

4.6 Effects of advection in the wall rock

Heat advection in the wall rock and the associated thermal recharge of the vane can be due either to the natural background flow of groundwater or to the injection and withdrawal of water, which causes a circulation around the vane.

In order to assess the impact of natural background flow on the thermal, advective recharge of RAD-EGS, we increased the background basin-wide hydraulic gradient i from 0.2% to 5%, which is a value similar to that reported in a study of a hydrothermal system in West Virginia (Perry et al. 1979). Even with this increase the production temperature does not change much relative to the base case (see **Fig. 8a**). This insensitivity can be explained by estimating the flow rate of relatively hot groundwater through the vane due to natural background flow relative to the imposed flow rate of the relatively colder injection water. The background mass flux through the vane is, according to Darcy's law, approximately given by

$$\dot{m}_{back} = h_{vane}\, l_{vane}\, \frac{\kappa_{sed}\, \rho_f^2\, g}{\mu}\, i \qquad (12)$$

where the simplifying assumptions are made that (a) the increased vane permeability does not significantly affect the flow relative to the background flow in the nonstimulated HSA, and (b) the temperature-dependent water density ρ_f and dynamic viscosity μ are constant or taken as averaged values. For an assumed average water/rock temperature of 200°C, $\mu = 0.14 \times 10^{-3}$ kg/m-s and ρ_f = 864 kg/m^3, and hence $\dot{m}_{back}$ = 1 kg/s which is only a 100th of the coolant flow rate. This explains why a 10-fold increase of the hydraulic gradient i does not significantly affect the production temperature. Also the pressure difference necessary to drive the flow in the vane is not much affected (see **Fig. 8b**).

For a tenfold higher HSA permeability, $\kappa_{sed} = 10^{-13}$ m^2, the rate of background flow is further increased to $\dot{m}_{back}$ = 10 kg/s, which now amounts to 1/10th of the coolant flow rate. However, this increased HSA permeability and hence smaller viscous resistance also allows the dense cold injected water to penetrate into the HSA portion below the vane. This deeper penetration, nevertheless, now hinders the, cold injected water from reaching the top of the vane as illustrated in **Fig. 9**. Thus, the lifetime of RAD-EGS is substantially prolonged through this density-driven flow relative to the base case as shown in **Fig. 8a**. And because of the overall higher transmissivity of the combined vane-wall rock system, the pressure difference needed to drive the flow is lower than for the base case (see **Fig. 8b**).

In order to elucidate the effects of a surrounding conductive aquifer, the aquifer permeability was set to the very small value of $\kappa_{sed} = 5\times10^{-15}$ m^2. This is similar to the scenario used in the JASON report to estimate the lifetime of a geothermal reservoir (JASON 2013). Thermal recharge of the vane primarily occurs through heat conduction from the surrounding wall rock. As a result, the cooling front moves more quickly upward as illustrated in **Fig. 10** relative to the base case shown in **Fig. 3b**. Thermal recharge through advective heat flow from the wall rock into the vane therefore substantially prolongs the lifetime of RAD-EGS as shown in **Fig. 8a**. At the same

time, the pressure difference needed to drive the flow through the vane increases as κ_{sed} and the transmissivity of the combined vane-wall rock system are decreased (see **Fig. 8b**).

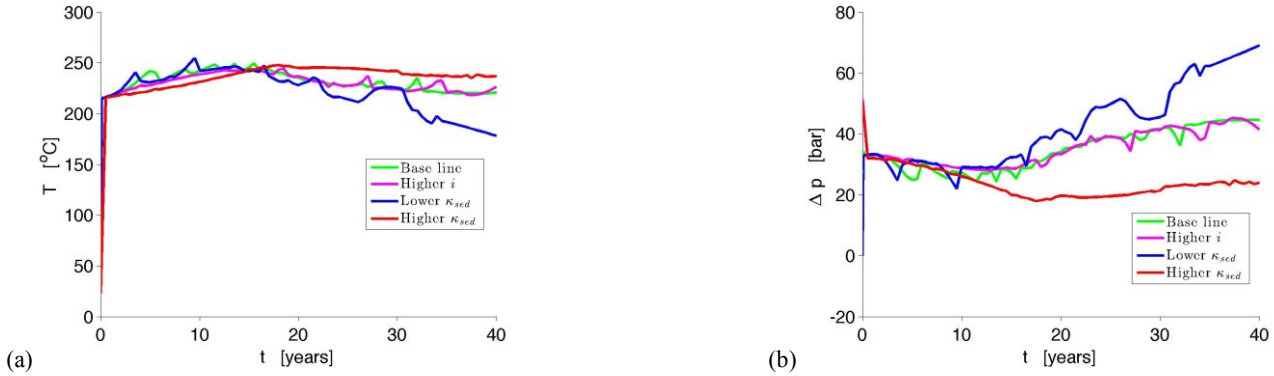

(a) (b)

Figure 8: (a) Effluent temperature and (b) pressure difference between the heads of the injection and production wells for the first (baseline) and last three simulation scenarios from Table 2.

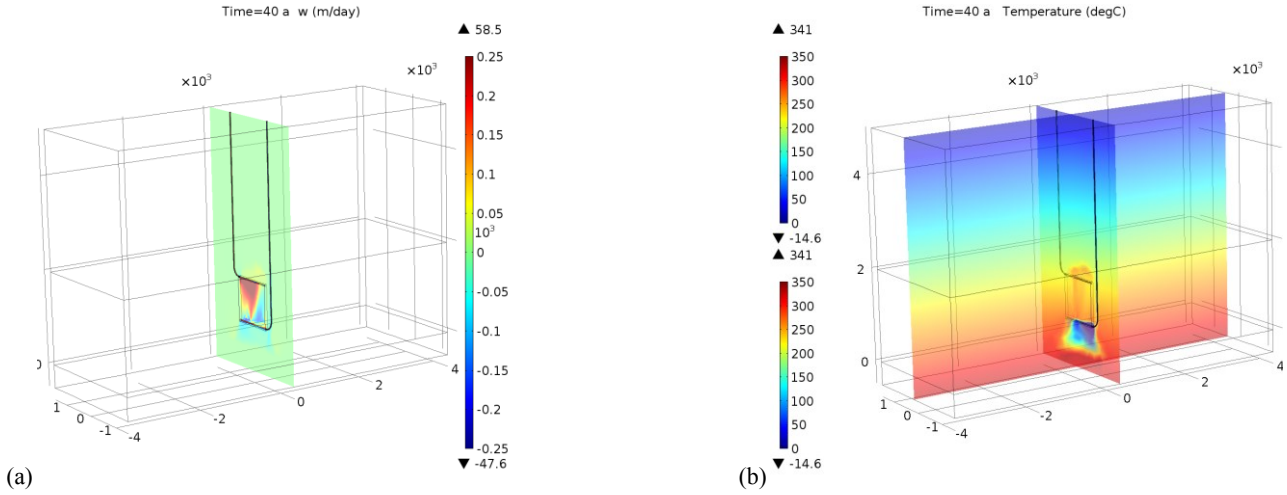

(a) (b)

Figure 9: For a higher HSA permeability, the injected coolant is able to penetrate the HSA underneath the vane, and the injected cold water is hindered from reaching the production well. (a) Vertical flow velocity in a slice through the vane 40 years after operation of RAD-EGS started. (b) Temperature in the same slice.

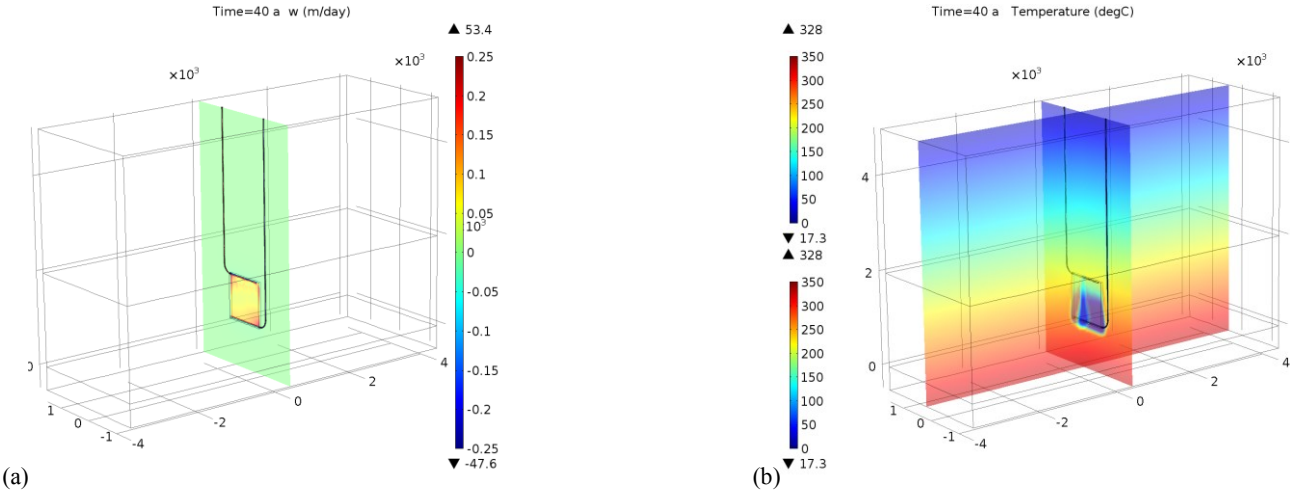

(a) (b)

Figure 10: For a lower HSA permeability, the injected coolant does not significantly penetrate the HSA underneath the vane, and thermal recharge of the vane is primarily due to heat conduction from the wall rock. (a) Vertical flow velocity in a slice through the vane 40 years after operation of RAD-EGS started. (b) Temperature in the same slice and a slice along the direction of background flow.

5. DISCUSSION AND SUMMARY

Nature has long solved the problem of efficiently and abundantly extracting Geothermal Energy and mankind has developed to a high art form the design and functioning of heat exchangers, of which one of the best is the combustion engine radiator. The careful construction of a Radiator style Enhanced Geothermal System (RAD-EGS) is at the core of opening the world to a clean, endless supply of energy. The primary intention of the present study is to investigate the viability of such a system in light of the long-term production of clean energy. We have thus performed numerical simulations in order to understand better the heat-transfer characteristics of RAD-EGS. We found that it is beneficial to emulate natural hydrothermal systems, in which hot fluids typically rise along vertical or near-vertical zones of high permeability and are recharged by larger scale regional flows. Operating RAD-EGS in natural "upward flow mode" not only requires less pumping power, but it also decreases thermal drawdown, because hydraulic short-circuiting is avoided within the vane.

Upward flow in the vane may be associated with a convective instability or not. The onset of convection depends on the magnitude of the Rayleigh number Ra, which is near critical here. The main parameters that determine the value of Ra in RAD-EGS are the vane height and the geothermal gradient. No matter whether convection occurs or not, a relatively sharp cooling front propagates upward through the vane, and hydraulic short-circuiting does not occur, unlike for induced downward flow.

The RAD-EGS is broadly similar to the EGS studied by Bataille et al. (2006). Their EGS consists of a fractured reservoir that was 750 m high, 750 m long and 35 m thick, which are dimensions that roughly agree with those of the radiator vane used in our study. However, the injection and production wells were vertical and abutted the reservoir on top of the two thin sidewalls. Their numerical simulations showed that early breakthrough of cold water occurred when the injection rate was too high and when convection did not occur because of a too small Rayleigh number. RAD-EGS does not appear to have such limitations, because cold fluid is injected at the bottom of the reservoir (vane) and produced on top.

The induced upward flow in the vane further delays thermal depletion of the geothermal reservoir if the injected, cold water moves downward into the rock formation underlying the vane. It is noteworthy that downward flow of injected cold water into the rock formation beneath the vane would, in the context of EGS built in hot dry rock (HDR), be labeled as a water loss occurring to the far field (Tester et al. 2006). Such losses are substantial and occur frequently in HDR, for example, in Fenton Hill (Brown 1988), Hijiori (Kawasaki et al. 2002) and Ogachi (Hori et al. 1999). These losses typically increase with increasing fluid injection pressure and hence flow rate, because the increased pressure may open up old fractures through which more water is lost. If loss of fluid to the reservoir occurs, more fluid must be added to the system. This is undesirable for several reasons: (1) water is expensive; (2) added water is not necessarily in chemical equilibrium with the reservoir rock, causing either dissolution of deposition of minerals in the rock or the borehole casing; and (3) makeup water is typically colder than water injected directly from the surface plant, decreasing the lifetime of an EGS (Tester et al. 2006). In strong contrast to HDR, in RAD-EGS water loss does not occur. This is because the RAD-EGS is built in wet rock, i.e., in sedimentary aquifers, which by definition are already saturated with water. Building an EGS in an aquifer also has the additional advantage that heat from the surrounding wall rock aquifer can be harvested through heat advection and not simply just by the gradually slowing heat conduction that leads to increasingly large cool thermal halos.

A possibly full-scale verification of this proposed Radiator-style EGS occurred in the experiment conducted at Fenton Hill by the Los Alamos National Laboratory between 1977 and 1986. This experiment was designed to test the conventional hot dry rock EGS style of energy extraction by drilling to over 8000 feet in the Jemez Mountains of north-central New Mexico where temperatures of over 180°C were found. Although drilling was designed to develop a more or less spherical zone of high permeability, hydrofracking stimulated and dilated a pre-existing near–vertical joint of "vanishingly small" flow impedance. Following flow testing for 75 days in early 1978, further stimulation opened a second set of near vertical joints in an oblique orientation to the initial vertical joint. The early phase produced thermal energy at 4MW for 75 days and the later phase at an equivalent of 10 MW. The overall near vertical vane-style character of the heat exchanger in this experiment is remarkably similar to that suggested for the RAD-EGS, which in lieu of a full scale test of the RAD-EGS serves' as an indication of its likely feasibility.

The key to emulating Natural Geothermal Systems is surgically building a tall, fracture-laden sheet-like network in hot wet rock basins, of which there is a worldwide abundance. In Earth surgery, like any surgery, two things are crucial. First, each incision or fracture must be precisely made, and, second, each incision must be precisely located through imaging. Precisely fracturing rock in the proper orientation, taking advantage of Sh_{max} and S_1 (vertical) in the local crust, and at the necessary intensity involves quickly stressing the rock beyond its natural strength, which can only be achieved by unconventional propellant fracking. In striking contrast to hydraulic fracking, solid propellant is capable of rapid, precisely controlled stress application involving essentially no introduced water. And the necessary highly detailed imaging is available from the Oil and Gas Industry, which works best in exactly these environments. All the critical ingredients: design, theory, and locations, like Colorado's Raton Basin, are in place to manufacture and test the RAD-EGS.

REFERENCES

Bachler, D. and T. Kohl (2005). "Coupled thermal-hydraulic-chemical modelling of enhanced geothermal systems." Geophysical Journal International **161**(2): 533-548.

Bataille, A., P. Genthon, et al. (2006). "Modeling the coupling between free and forced convection in a vertical permeable slot: Implications for the heat production of an Enhanced Geothermal System." Geothermics **35**(5-6): 654-682.

Brown, D. W. (1988). Anomalous earth stress measurements during a six-year sequence of pumping tests at Fenton Hill, New Mexico. Los Alamos National Laboratory report.

Caine, J. S. and S. R. A. Tomusiak (2003). "Brittle structures and their role in controlling porosity and permeability in a complex Precambrian crystalline-rock aquifer system in the Colorado Rocky Mountain Front Range." Geological Society of America Bulletin **115**(11): 1410-1424.

Cheng, P. and W. J. Minkowycz (1977). "Free Convection About a Vertical Flat-Plate Embedded in a Porous-Medium with Application to Heat-Transfer from a Dike." Journal of Geophysical Research **82**(14): 2040-2044.

Cuderman, J. F. (1984). High energy gas fracturing development-Final report to Gas Research Institute. Albuquerque, NM, Sandia National Laboratories.

Dempsey, D., S. Kelkar, et al. (2015). "Numerical modeling of injection, stress and permeability enhancement during shear stimulation at the Desert Peak Enhanced Geothermal System." International Journal of Rock Mechanics and Mining Sciences **78**: 190-206.

Denlinger, R. P. and R. L. Kovach (1981). "3-Dimensional Gravity Modeling of the Geysers Hydrothermal System and Vicinity, Northern California." Geological Society of America Bulletin **92**(6): 404-410.

Diersch, H. J., O. Kolditz, et al. (1989). "Finite-Element Analysis of Geothermal Circulation Processes in Hot Dry Rock Fractures." Zeitschrift Fur Angewandte Mathematik Und Mechanik **69**(3): 139-153.

Dzikowski, M., J. Y. Josnin, et al. (2016). "Thermal Influence of an Alpine Deep Hydrothermal Fault on the Surrounding Rocks." Groundwater **54**(1): 55-65.

Fairley, J. P., S. E. Ingebritsen, et al. (2010). "Challenges for Numerical Modeling of Enhanced Geothermal Systems." Ground Water **48**(4): 482-483.

Freeze, R. A. and J. A. Cherry (1979). Groundwater. Englewood Cliffs, N.J., Prentice-Hall.

Fu, F. Q., B. I. A. McInnes, et al. (2010). "Numerical modeling of magmatic-hydrothermal systems constrained by U-Th-Pb-He time-temperature histories." Journal of Geochemical Exploration **106**(1-3): 90-109.

Geiser, P., Marsh, B., and Hilpert, M. (2015a). Method for a Radiator EGS To harvest geothermal energy. USA.

Geiser, P., Marsh, B., and Hilpert, M. (2015b). The Radiator-EGS System: A fresh solution to geothermal heat extraction. Fourtieth Workshop on Geothermal Reservoir Engineering Stanford University. Stanford, CA.

Homsy, G. M. and A. E. Sherwood (1976). "Convective Instabilities in Porous-Media with through Flow." AICHE Journal **22**(1): 168-174.

Hori, Y., K. Kitano, et al. (1999). "Present status of the Ogachi HDR Project, Japan, and future plans." Geothermics **28**(4-5): 637-645.

JASON (2013). Enhanced Geothermal Systems. Washington, DC, The MITRE Corporation. **JSR-13-320**.

Jones, M. C. and J. M. Persichetti (1986). "Convective Instability in Packed-Beds with Throughflow." AICHE Journal **32**(9): 1555-1557.

Kawasaki, K., Y. Oikawa, et al. (2002). Heat extraction experiment at Hijiori test site (first year). Twenty-Seventh Workshop on Geothermal Reservoir Engineerining, Stanford, CA.

Lapwood, E. R. (1948). "Convection of a Fluid in a Porous Medium." Proceedings of the Cambridge Philosophical Society **44**(4): 508-521.

Malkovsky, V. I. and A. A. Pek (2015). "Onset of Fault-Bounded Free Thermal Convection in a Fluid-Saturated Horizontal Permeable Porous Layer." Transport In Porous Media **110**(1): 25-39.

Murphy, H. D. (1979). "Convective Instabilities in Vertical Fractures and Faults." Journal of Geophysical Research **84**(Nb11): 6121-6130.

Nield, D. A. and A. Bejan (2006). Convection in porous media. New York, Springer.

Perry, L. D., J. K. Costain, et al. (1979). "Heat-Flow in Western Virginia and a Model for the Origin of Thermal Springs in the Folded Appalachians." Journal of Geophysical Research **84**(Nb12): 6875-6883.

Ratouis, T. M. P. and S. J. Zarrouk (2016). "Factors controlling large-scale hydrodynamic convection in the Taupo Volcanic Zone (TVZ), New Zealand." Geothermics **59**: 236-251.

Stimac, J. A., F. Goff, et al. (2001). "Thermal modeling of the Clear Lake magmatic-hydrothermal system, California, USA." Geothermics **30**(2-3): 349-390.

Tester, J. W., B. J. Anderson, et al. (2006). The future of geothermal energy: Impact of enhanced geothermal systems (EGS) on the United States in the 21st Century, Massachusetts Institute of Technology.

Watanabe, N., B. Zehner, et al. (2011). "Numerical analysis and visualization of uncertainty effects in thermo-hydro-mechanical coupled processes in a hot-dry-rock geothermal reservoir." Calibration and Reliability in Groundwater Modelling: Managing Groundwater and the Environment **341**: 57-62.